

GT2011-45++'

INJECTION OF SUBCRITICAL AND SUPERCRITICAL AVIATION KEROSENE INTO A HIGH-TEMPERATURE AND HIGH-PRESSURE CROSSFLOW

Xin Xue

National Key Laboratory of Science and
Technology on Aero-Engine Aero-
thermodynamics, School of Jet Propulsion, Beijing
University of Aeronautics and Astronautics
Beijing, 100191, P. R. CHINA
Email: xuexin@sjp.buaa.edu.cn

Wei Gao

The 11th Research Institute of CASC
Xi'an, Shaanxi, 710000, P. R. China
Email: buaa_gaowei@163.com

Quanhong Xu

National Key Laboratory of
Science and Technology on Aero-
Engine Aero-thermodynamics,
School of Jet Propulsion, Beijing
University of Aeronautics and
Astronautics
Beijing, 100191, P. R. CHINA
Email: xuquanhong@buaa.edu.cn

Yuzhen Lin

National Key Laboratory of
Science and Technology on
Aero-Engine Aero-
thermodynamics, School of Jet
Propulsion, Beijing University
of Aeronautics and
Astronautics
Beijing, 100191, P. R. CHINA
Email: linyuzhen@buaa.edu.cn

Chih-Jen Sung

Department of Mechanical
Engineering, University of
Connecticut
Storrs, CT 06269, USA
Email: cjsung@engr.uconn.edu

ABSTRACT

In the present experimental study, injection of subcritical and supercritical kerosene into a high-temperature and high-pressure subsonic crossflow was investigated. Visualization and characterization of the jet structures were performed using schlieren imaging, from which the jet penetration trajectory was determined. For the conditions tested, a correlation of jet penetration trajectory was developed, with momentum ratio as the primary parameter. An analysis based on one-dimensional isentropic flow was also conducted to calculate the flow parameter variations in the nozzle and along the jet trajectory. Using a three-component kerosene surrogate, the phase transition processes for supercritical and subcritical kerosene jets were illustrated in the thermodynamic phase diagram. Experimental and analytical results demonstrated that the behavior and penetration of supercritical kerosene injection into high temperature and high pressure crossflow were closer to those of the case with gas jet injecting into a gas crossflow than the case with liquid kerosene injection.

INTRODUCTION

Investigation of subcritical and supercritical fluid injected into high temperature and high pressure crossflow has attracted significant attention because of its relevance to the development of advanced propulsion systems [1]. For advanced gas turbine technologies, scramjet applications, and pulse detonation engine concepts, the hydrocarbon fuels are used as primary coolant to cool the airframe and engine components [2]. In these applications, as the fuel absorbs heat from the wall, the fuel temperature can be increased beyond its critical value. Additionally, the fuel injection pressure is normally higher than the fuel critical pressure. Thus, in a regenerative cooling system the fuel can become supercritical before injection into combustor. Note that the fuel distribution in air-breathing propulsion systems can have a significant effect on combustion stability, efficiency and emissions [3-5]. It is also known that supercritical fuels exhibit unique thermophysical and transport properties, such as liquid-like density, gas-like diffusivity, zero latent heat, zero surface tension, and large

compressibility [6,7]. In addition, jet fuels have complex variations in specific heat, speed of sound, viscosity, thermal conductivity, and mass diffusivity with increasing temperature, and typically have sharp property value changes at a temperature near the critical point [3-6].

Significant work has been done on subcritical and supercritical fuel injection, including supercritical injection processes of lower-order hydrocarbons in quiescent environments [2,8-11]. These studies indicated thermodynamic anomalies near the critical point and visible shock structure. Doughthip *et al.* [12] studied the jet structure, penetration distance, and cone angle of supercritical Jet-A injected into a supercritical environment filled with nitrogen.

Stenzler *et al.* [13] investigated the penetration of distilled water, acetone, and 4-heptanone jets into a gaseous crossflow with temperatures up to 300 °C at atmospheric pressure. Penetration results were correlated with momentum flux ratio, Weber number, and liquid viscosity over the range of conditions studied. Wu *et al.* [14,15] experimentally studied the breakup processes of water and ethyl alcohol jets injected into subsonic air crossflows. A correlation of liquid column trajectories with liquid/air momentum flux ratios was conducted based on a force analysis of a cylindrical liquid element subjected to an aerodynamic drag force.

Corn *et al.* [16] conducted an experiment to characterize a superheated Jet-A jet injected into an unheated crossflow. The explosive breakup that was seen in the flash-atomized spray produced sub-micron droplets with a high radial and transverse momentum that resulted in an increasing fuel vapor concentration for the same penetration distance when compared with the shear-atomized case. This unique behavior makes superheated fuels an attractive design feature for fuel preparation devices that can employ flash boiling to enhance fuel atomization and mixing in a compact volume.

In view of very limited studies on the injection of supercritical and subcritical jet fuel into elevated temperature and pressure subsonic crossflow, the present investigation aimed to provide such experimental data over a wide range of conditions. Specifically, in this study RP-3 aviation kerosene was injected into a subsonic crossflow at fuel temperatures of 500–700 K and injection pressures of 1.5–4.0 MPa. The temperatures, pressures, and velocities of air crossflow were in the range of 290–680 K, 1.0–2.2 MPa, and 70–75 m/s, respectively. As such, the present test conditions allowed the comparison of injection phenomena for supercritical fuel as well as subcritical vaporized fuel. Characterization of the jet structure was performed using schlieren imaging technique. Based on the schlieren image of jet-crossflow interaction, the jet penetration distance was then determined. Jet penetration trajectories obtained at varying conditions were further correlated to identify the controlling factor. Experimental results using subcritical and supercritical kerosene injection were compared with other injection schemes discussed in the literature as well.

NOMENCLATURE

| | | |
|------------|--|-------------------|
| A | area | mm ² |
| B | blue value | |
| d | nozzle diameter | mm |
| F | function | |
| g | gray level | |
| G | green value | |
| H | total enthalpy | kJ/kg |
| h | enthalpy | kJ/kg |
| J | momentum flux ratio, $\rho_j V_j^2 / \rho_a V_a^2$ | |
| k | specific heat ratio | |
| L | length of jet trajectory | mm |
| \dot{m} | mass flow rate | kg/s |
| P | pressure | MPa |
| Q | compression factor | |
| R | red value | |
| s | entropy | kJ/(kg·K) |
| T | temperature | K |
| V | velocity | m/s |
| X | length direction of test section | mm |
| Y | height direction of test section | mm |
| Z | nozzle axis | mm |
| ρ | density | kg/m ³ |
| Subscripts | | |
| a | crossflow property | |
| c | critical property | |
| i | an point at axis | |
| j | jet property | |
| m | maximum | |
| p | pressure function | |
| s | entropy function | |
| v | velocity function | |
| ρ | density function | |
| 1 | starting point of nozzle convergent section | |
| 2 | nozzle exit | |

EXPERIMENTAL SPECIFICATIONS

Figure 1 shows the fuel injection system and the schlieren imaging setup. The fuel injection system consists of a fuel tank, a compressed air bottle, a two-stage fuel heater, a fuel temperature control unit, and an injector. The fuel tank had an internal volume of 1000 liters. This large volume is necessary for long duration experiments and to minimize the injectant pressure variations during injection. A coriolis-type mass flow meter with a measurement range of 1–10 g/s and an uncertainty of less than $\pm 1\%$ was used in the present study to determine the fuel mass flow rate. The fuel was pumped into a two-stage heater to gradually reach the selected temperature. The first-stage heater consisted of a 2 m long stainless steel tube of 2 mm inner diameter and 0.2 mm wall thickness, which was electrically heated by directly passing 50–60 volts AC across the tube. This first-stage heater can heat kerosene of 3 g/s up to

520 K with negligible coking deposits. The second-stage heater had the same structure and heating method as the first-stage one, while its heating voltage was 60–85 volts AC, capable of rapidly heating kerosene to 750 K. The residence time of heated kerosene within the second-stage heater was typically less than 4 s, thereby minimizing the extent of fuel coking. A fuel temperature control unit was used to control the injection temperature of the test fluid by changing the heating power of the fuel heater. After each run, air was used to purge the fuel heater to avoid carbon deposit accumulation caused by residual fuel.

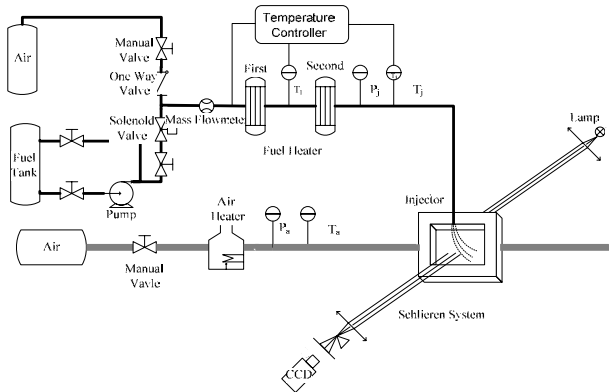


Fig. 1 Schematic of fuel injection system and schlieren imaging setup.

The crossflow air was established using a high pressure air tank capable of delivering 1.5 kg/s at 5 MPa at the tank outlet. The air flow rate was metered with an orifice with 1% accuracy. Through a heat exchanger, the air flow can be heated up to 700 K. The crossflow temperature (T_a) and pressure (P_a) were based on the measured values upstream of the test section passage, respectively using a K-type thermocouple with an uncertainty of ± 5 K and a pressure transducer with an uncertainty of ± 0.1 KPa.

The test section consisted of a transition section that converted a round inlet pipe to square tunnel with inner dimensions of 70 mm \times 25 mm. The test section was mounted vertically such that the air flowed downward. A honeycomb was also used to produce a uniform crossflow of air across the square tunnel. Quartz windows (60 mm \times 60mm) were installed to allow optical access.

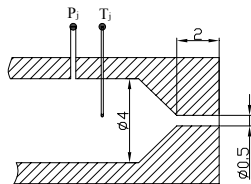


Fig. 2 Schematic of injector assembly. Length dimensions are in mm.

The test fluid was injected into a crossflow through an injector nozzle assembly shown in Fig. 2 to study the effects of fuel temperature and pressure on jet structure and phase transition process. The exit diameter of the injector was $d=0.5$ mm, and the ratio of passage length to exit diameter was 4, as illustrated in Fig. 2. The fuel injection temperature T_j and pressure P_j were monitored upstream of the injector passage using a K-type thermocouple with an uncertainty of ± 5 K and a pressure transducer with an uncertainty of ± 0.1 KPa, respectively. In the following discussion, the readings of T_j and P_j are used to represent jet properties.

Visualization of the jet structure and the jet phase transition was accomplished with schlieren photographs. The schlieren imaging system included a halogen lamp, two 200 mm diameter parabolic mirrors with focal length of 2000 mm, and a Nikon D300 camera with a shutter speed of 1/25 s. This arrangement provided an image magnification of 2.5 and a field of view of 9.5 mm \times 6.4 mm covering 100 d downstream of the injector.

Table 1 Summary of test conditions

| Parameter | Range |
|-----------|-------------|
| P_j | 1.5–4.0 MPa |
| T_j | 500–700 K |
| P_a | 1.0–2.2 MPa |
| T_a | 290–680 K |
| V_a | 70–75 m/s |

Table 2 Selected test conditions

| Case | P_j [MPa] | T_j [K] | P_a [MPa] | T_a [K] | V_a [m/s] | J |
|------|----------------|--------------|----------------|--------------|----------------|----|
| 1 | 2.53 | 653 | 2.0 | 633 | 70 | 17 |
| 2 | 2.20 | 620 | 2.0 | 633 | 70 | 8 |
| 3 | 2.84 | 652 | 2.0 | 633 | 70 | 24 |
| 4 | 2.20 | 650 | 2.0 | 633 | 70 | 8 |
| 5 | 3.05 | 660 | 2.0 | 678 | 73 | 28 |
| 6 | 3.05 | 660 | 2.0 | 653 | 73 | 27 |

Table 1 summarizes the present test conditions, covering fuel states from subcritical to supercritical. Note that the critical pressure and critical temperature of RP-3 aviation kerosene are $P_c=2.21$ MPa and $T_c=630$ K, respectively. The fuel injection pressures were in the range of $P_j=1.5$ –4.0 MPa, yielding reduced injection pressure from 0.68 to 1.81. Moreover, temperatures of the fuel jet were varied from 500 to 700 K, resulting in reduced temperatures from 0.79 to 1.11. The crossflow pressures and temperatures were in the range of $P_a=1.0$ –2.2 MPa and $T_a=290$ –680 K, respectively. Note that the crossflow pressures tested were smaller than the critical

pressure of RP-3 while the highest crossflow temperature used was higher than the critical temperature of RP-3. The crossflow was subsonic with velocities ranging from 70 to 75 m/s.

Table 2 further lists the temperature/pressure conditions of the fuel and the crossflow air as well as the momentum ratios for selected cases. Note that the fuel injection conditions were supercritical for Cases 1, 3, 5, and 6, while those of Cases 2 and 4 were subcritical.

RESULTS AND DISCUSSION

Jet Behavior

Figure 3(a) shows a schlieren image for a supercritical RP-3 injection with $P_j=2.84$ MPa and $T_j=652$ K into a crossflow of $P_a=2.0$ MPa, $T_a=633$ K, and $V_a=70$ m/s, while Fig. 3(b) is for a subcritical RP-3 injection with $P_j=2.20$ MPa and $T_j=620$ K. It is seen that both supercritical and subcritical fuel jets when injecting into high temperature and pressure crossflow appear like a typical jet in crossflow. The crossflow causes the column to bend and flatten in the leeward direction. However, momentum and heat exchanges between the kerosene jet and the mainstream are expected to affect the phase transition of kerosene. Because the current crossflow was at high pressure, before interacting with the crossflow the heated fuel jet did not expand rapidly outwards upon injection. Such a rapid expansion, on the other hand, was observed in the flashing atomization study of Corn *et al.* [16], in which the superheated Jet-A at fuel temperature of 513 K was injected into an atmospheric crossflow. The fuel temperature and pressure as well as crossflow temperature and pressure of Corn *et al.* [16] were much lower than current study. Thus, the jet behaviors of supercritical and subcritical kerosene injecting into elevated temperature/pressure crossflow are different from those of the liquid fuel jet and the flashing atomization.



(a) $P_j=2.84$ MPa and $T_j=652$ K.



(b) $P_j=2.20$ MPa and $T_j=620$ K.

Fig. 3 Schlieren images of RP-3 jets. The crossflow conditions are $P_a=2.0$ MPa, $T_a=633$ K, and $V_a=70$ m/s.

Determination of Penetration Distance

For the schlieren system, variations in the index of refraction due to density gradients in the fluid cause the collimated light passing through to be deflected. This distortion creates a spatial variation in the light intensity, which can be visualized directly in a schlieren photograph. Since the fuel injection density is substantially different from the gaseous crossflow density in the current study, the light intensity of the fuel jet in the schlieren photograph (cf. Fig. 3) can be used to characterize the penetration distance. Here, the penetration distance was defined as the distance from the upper surface of the jet to the bottom wall of the tunnel.

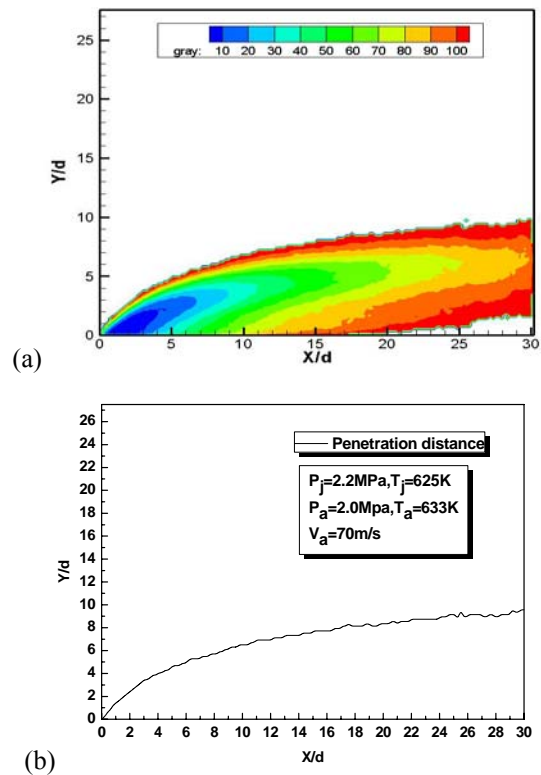


Fig. 4 Determination of RP-3 jet penetration distance.

Specifically, the gray level distribution of schlieren photograph was obtained using the pixel RGB values. The pixel gray values were determined as a function of the RGB values according to

$$g = 0.3R + 0.6G + 0.1B . \quad (1)$$

Based on Eq. (1), the gray level distribution of a photograph can be obtained, as shown in Fig. 4(a). Further, gray levels greater than 80% of the average gray level in a given photograph were ignored, as this somewhat arbitrary cutoff generally corresponded well with visualization for the conditions tested. By tracing the locus of the maximum Y with

gray level below the cutoff along the jet flow direction and taking the nozzle exit as the start point, as plotted in Fig. 4(b), the jet penetration distance can be determined. This determination of penetration was further validated by comparing with the maximum penetration data of Wang and Yu [17] and Kush and Schetz [18]. The comparison shown in Fig. 5 demonstrates that the results deduced using the current method agree well with the literature data, thereby indicating the adequacy of the underlying methodology.

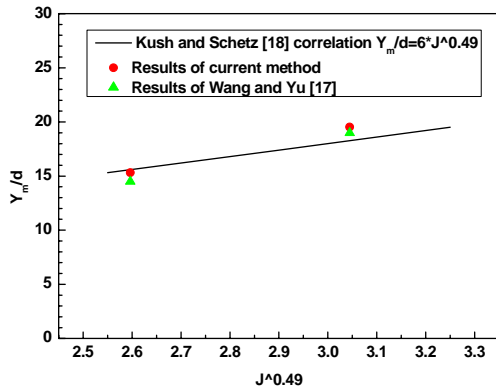


Fig. 5 Validation of the current method of penetration determination by comparing with the literature data.

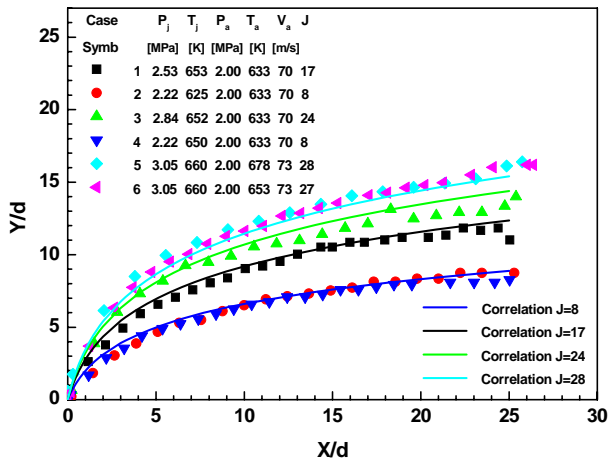


Fig. 6 Comparison of experimental and correlated jet penetration trajectories at varying test conditions.

Jet Penetration and Correlation

Following the penetration determination illustrated in Fig. 4, Fig. 6 plots the experimental penetration traces (denoted as symbols) of RP-3 kerosene jets at varying test conditions listed in Table 2. With the same injector diameter, Fig. 6 shows that the penetration of supercritical and subcritical kerosene injection into a crossflow depends on the momentum flux ratio.

Specifically, the penetration height increases with increasing momentum ratio, as expressed in the following correlation:

$$\frac{Y}{d} = 1.05J^{0.44} \ln\left(1 + 1.14 \frac{X}{d}\right). \quad (2)$$

Figure 6 further compares experimental (symbols) and correlated (lines) penetration traces at varying conditions. The correlation of Eq. (2) generally well represents the experimental results.

Comparison with Liquid and Gas Jets

Figure 7 shows the comparisons of the current experimental results, the trajectories predicted by the correlations for liquid kerosene [19,20] and gas [21] jets in a crossflow, and the experimental results of Ref. [16]. The correlations of Refs. [19,20] were derived from PDDA measurements and laser-sheet imaging technique of Jet-A injected into a crossflow under atmospheric temperature, while the correlation of Lefebvre [21] was derived from injecting air into an air crossflow under atmospheric temperature and pressure. Additionally, the penetrations of Refs. [19,21] and Refs. [16,20] were defined as the distance between the bottom of the tunnel and the centerline of the jet and the distance between the upper surface of the spray and the bottom of the tunnel, respectively.

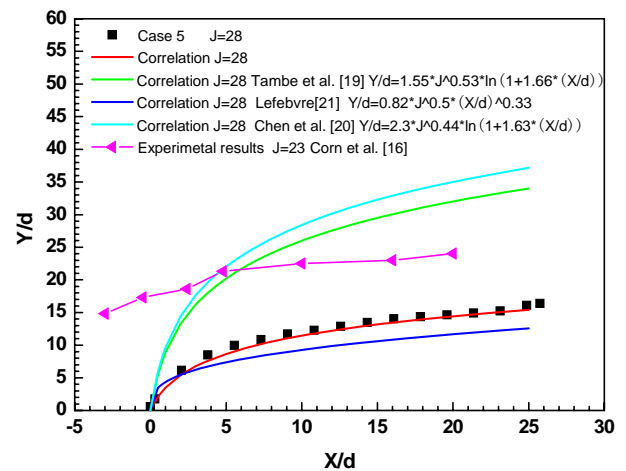


Fig. 7 Comparison of the current penetration trajectory results and the literature data [16, 19-21].

It is seen from Fig. 6 that the correlations of Tambe *et al.* [19] Chen *et al.* [20] over-predicts the current data by more than 120%, while that of Lefebvre [21] under-predicts by ~20%. When comparing with the experimental results of Corn *et al.* [16] for Jet-A injection into an atmospheric crossflow, the maximum spray penetration of their high speed video imaging measurements was used. Flash atomization resulted from the

rapid expansion of vapor bubbles in the fuel, which caused the fuel to shatter upon injection [16]. As a reference, the injection temperature and pressure of Jet-A in Ref. [16] were 0.673 MPa and 540 K, respectively. Because the results of Corn *et al.* [16] were related to the so-called flashing atomization, the jet penetration distance of superheated fuel was much higher than the current data. As such, the comparison shown in Fig. 7 indicates that the penetration distance of supercritical injection was somewhere between those of liquid jet, flashing atomization, and gas jet. The penetration distance of supercritical injection was much closer to the gas jet than liquid jet and flashing atomization.

In order to provide insight into the injection processes of kerosene observed in different injection regimes, the thermophysical properties of RP-3 fuel at different pressures and temperatures are needed. Since aviation kerosene could have hundreds of hydrocarbon components [22], in order to simplify the calculations of thermophysical properties, it is useful to employ a surrogate fuel that emulates the real fuel characteristics, yet with fewer hydrocarbon components.

Table 3 Composition (mass basis) of RP-3 Aviation Kerosene

| Hydrocarbon | Mass Percentage [%] |
|-------------------------|---------------------|
| Saturated | |
| Alkanes | 52.2 |
| Naphthenes | |
| Monocyclic | 33.8 |
| Bicyclic | 6.0 |
| Tricyclic | 0.1 |
| Sub-total | 92.1 |
| Aromatic | |
| Alkyl benzenes | 5.1 |
| Indan and tetralin | 1.3 |
| Naphthalene | 0.6 |
| Naphthalene derivatives | 0.9 |
| Sub-total | 7.9 |
| Total | 100 |

Table 3 lists the measured mass percentages of various components in the RP-3 fuel employed herein. As suggested by Dagaut [23], a three-component surrogate mixture, consisting by mole of 49% n-decane, 44% 1,3,5-trimethylcyclohexane, and 7% n-propylbenzene, was chosen to calculate the representing thermodynamic properties of RP-3 kerosene fuel. The phase diagram of this three-component RP-3 kerosene surrogate obtained using SUPERTRAPP [24] developed by NIST (National Institute of Standards and Technology) are shown in Fig. 8. SUPERTRAPP [24] is an interactive computer database for the prediction of thermodynamic and transport properties of fluid mixtures. The pressure-temperature diagram in Fig. 8 depicts the saturated liquid and vapor boundaries, the

critical point, and the two-phase zone for the kerosene surrogate fuel. In addition, the fuel injection pressures and crossflow pressures for the current Case 5, Corn *et al.* [16], and Tambe *et al.* [19] are indicated in Fig. 8.

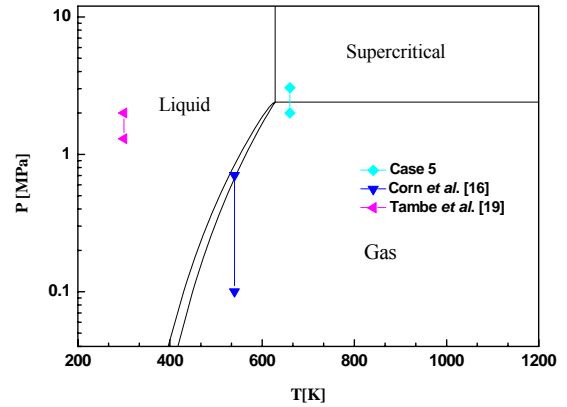


Fig. 8 Phase transition comparison for the present experimental data ($J=28$, $P_j=3.05$ MPa, $T_j=660$ K, $P_a=2.0$ MPa, $T_a=678$ K) and the literature data.

As shown in Fig. 8, while Case 5 was for supercritical injection, the final state was in the vapor phase. In the study of Tambe *et al.* [19], the fuel was in the liquid state for the entire injection process. For the study of Corn *et al.* [16], injection was seen to be from the two-phase zone to the vapor zone. However, Corn *et al.* [16] stated that the injection was from subcooled liquid to vapor phase. The discrepancy of the current two-phase zone and the stated subcooled liquid therein can be attributed to the different thermodynamic properties of the jet fuel used in the phase diagram calculations. Further, since the injection characteristics depend on the state of kerosene at the nozzle exit, in the following a one-dimensional analysis is introduced to calculate the fuel flow parameter variation along the jet trajectory.

ONE-DIMENSIONAL ANALYSIS

Analysis and Methodology

In order to understand the supercritical and subcritical kerosene flow in the nozzle, a one-dimensional analysis is proposed for such calculations. Figure 9 shows the schematic of the nozzle and the definitions of the relevant parameters. The Z coordinate is defined along the kerosene flow. The zero point (Point 1) is the intersection point of the convergent section and the constant area section, while the nozzle exit is denoted as Point 2. The inner nozzle part of the Z coordinate is along the nozzle axis, whereas the outer nozzle part of the Z coordinate is along the centerline of the kerosene trajectory.

Although the actual velocity at the nozzle exit is unknown, it is considered that the kerosene flow speed at the nozzle exit reaches the local sound speed. Different from the ideal gas,

supercritical fluid does not meet the ideal gas equation of state. In particular, compression factor Q is usually not unity. Additionally, both compression factor and specific heat ratio k are not constant and vary with temperature and pressure. Therefore, it is not possible to calculate temperature and pressure distribution of kerosene inside the nozzle using the ideal gas equations and ideal gas equation of state. Assumptions associated with the present analysis are discussed as follows.

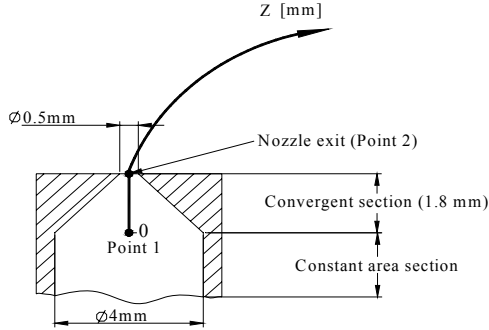


Fig. 9 Coordinate definition for the analysis.

It was assumed that the internal flow of kerosene is one-dimensional steady flow. Because the passage inside the nozzle is very short, less than 10 mm, and there are insulating materials outside the nozzle, the heat loss is negligible. Since the nozzle internal surface is smooth and has no sudden expansion section, the pressure loss is insignificant. As such, the internal kerosene flow was assumed to be an isentropic process. Based on the abovementioned assumptions, the variations of temperature, pressure, velocity, and density of kerosene can be calculated with given injection pressure and temperature.

As shown in Fig. 2, kerosene flow temperature and pressure were measured before the convergent section (before $Z=0$). The diameter ratio of the entrance and the exit of convergent section was 8, while the area ratio was 64. Since the speed of sound of supercritical kerosene is about 100 m/s and since the estimated velocity in the constant area section is within 1–2 m/s, the measured temperature and pressure in this section of nozzle were considered to be the corresponding total properties of kerosene.

Denoting pressure, temperature, velocity, entropy, enthalpy, and density at intersection point of the convergent section and the constant area section as P_1 , T_1 , V_1 , s_1 , h_1 , and ρ_1 , respectively, which are same to parameters in the constant area section; the corresponding parameters at the nozzle exit are designated as P_2 , T_2 , V_2 , s_2 , h_2 , and ρ_2 . According to the isentropic relation, the following holds:

$$s_1 = s_2 . \quad (3)$$

For one-dimensional isentropic flow, the total entropy is constant:

$$h_1 + \frac{1}{2}V_1^2 = h_2 + \frac{1}{2}V_2^2 . \quad (4)$$

Since there must be unique entropy and enthalpy for given pressure and temperature, the following equations are obtained:

$$h = F_h(P, T) \quad (5)$$

$$s = F_s(P, T) \quad (6)$$

$$\rho = F_\rho(P, T) . \quad (7)$$

Based on the above analysis, in the constant area section it was assumed that the kinetic energy as compared to the static enthalpy can be considered to be zero because of its low velocity, and hence V_1 can be considered as zero. As mentioned earlier, the velocity of supercritical kerosene at the nozzle exit (V_2) is assumed to be equal to the local speed of sound. As the speed of sound is also function of temperature and pressure, it can be expressed as:

$$V = F_v(P, T) . \quad (8)$$

However, the pressure and temperature at the nozzle exit need to be solved, because V_2 is still unknown.

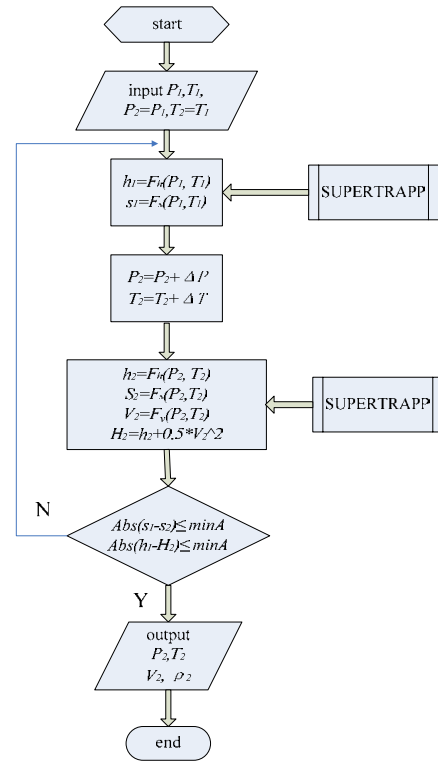


Fig. 10 Flow chart for solving fuel flow parameters at nozzle exit with given injection pressure and temperature.

With the measured values of P_1 and T_1 as well as $V_1 \approx 0$, s_1 and h_1 can be calculated by Eqs. (5) and (6). Although all the unknown parameters at the nozzle exit can be solved using the above equations, the fluid entropy, enthalpy, density, and speed of sound are implicit functions of temperature and pressure, and different functions have different coefficients, or even may have different forms. The SUPERTRAPP software [24] was employed to calculate the thermophysical properties of the three-component surrogate, including entropy, enthalpy, density and speed of sound. Therefore, in conjunction with the SUPERTRAPP software [24], temperature and pressure at the nozzle exit can be solved for given injection temperature and pressure. Subsequently, the exit parameters of kerosene can be determined. Detailed solution steps are highlighted in Fig. 10.

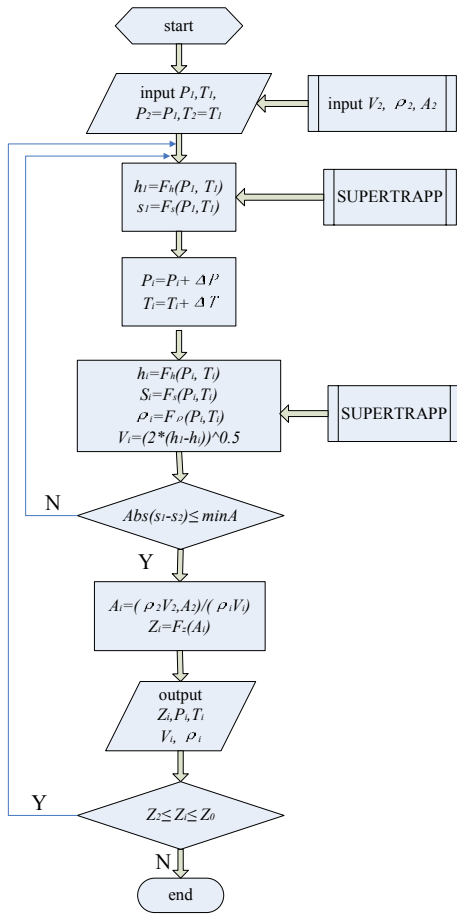


Fig. 11 Procedure for solving the state parameters at any point along the nozzle axis based on the injection pressure and temperature.

After obtaining the kerosene flow parameters at the nozzle exit, the mass flow rate of kerosene is determined. According to the mass continuity equation,

$$\dot{m}_1 = \dot{m}_i = \rho_i V_i A_i, \quad (9)$$

the parameters, including P_i , T_i , V_i , s_i , h_i , and ρ_i , at any cross-sectional area A_i can be related. In the case of a given nozzle shape, the relationship of the cross-sectional area and the coordinate Z can be also expressed as:

$$Z_i = F_z(A_i). \quad (10)$$

Using the above equations and SUPERTRAPP [24], the variations of the fuel state properties along the nozzle axis can be iteratively solved, as detailed in Fig. 11.

In order to demonstrate the viability of this one-dimensional model, supercritical ethylene injection process at the experimental condition in Ref. [2] was analyzed. Figure 12 compares the experimental data of Ref. [2] and the present calculated results, showing the maximum error is less than 8%. Also note that the maximum error occurs at the point where the pressure changes most sharply. In general, the present model captures quite well the experimental results qualitatively and quantitatively.

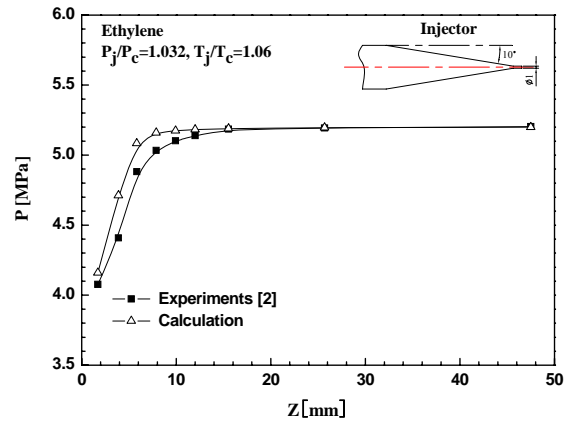


Fig. 12 Comparison of experimental [2] and calculated static pressure distributions in the nozzle for supercritical ethylene injection.

To further understand the phase transition process of kerosene jet, the fuel flow parameter variation along the jet trajectory, from injection into the crossflow to mixing with the air flow, needs to be determined. Using one-dimensional linear hypothesis, the temperature along the centerline of the kerosene jet penetration can be considered as a linear variation from the nozzle exit value (T_2) to the ambient value (T_a), as shown in Eq. (11), where L is the total length of the jet penetration and Z_i is a specific location along the trajectory of the jet penetration.

$$T_i = \frac{T_2 - T_a}{L} Z_i, \quad (11)$$

Similarly, for the present experimental conditions, the pressure variation along the penetration trajectory can be expressed as

Eq. (12), where P_2 is the jet pressure at the nozzle exit and P_a is the crossflow pressure,

$$P_i = \frac{P_2 - P_a}{L} Z_i. \quad (12)$$

Model Results and Discussion

Figures 13 and 14 respectively plot the variations of pressure and temperature of the kerosene flow along the nozzle axis and the jet trajectory centerline, for both Cases 4 and 5. In Figs. 13 and 14, the section of $Z=0-1.8$ mm is in the nozzle along the jet flow direction, while the section of $Z=1.8-12$ mm is along the jet penetration trajectory.

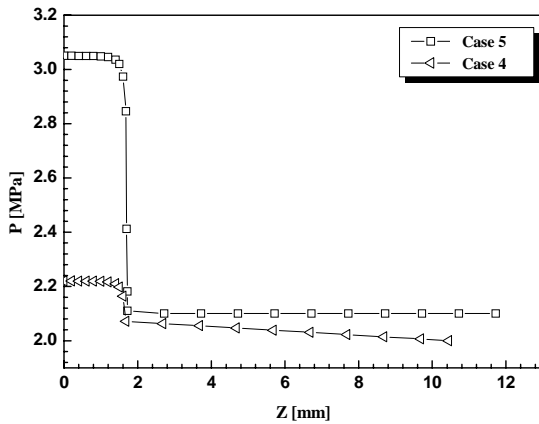


Fig. 13 Variation of jet pressure along the nozzle axis and the jet trajectory centerline.

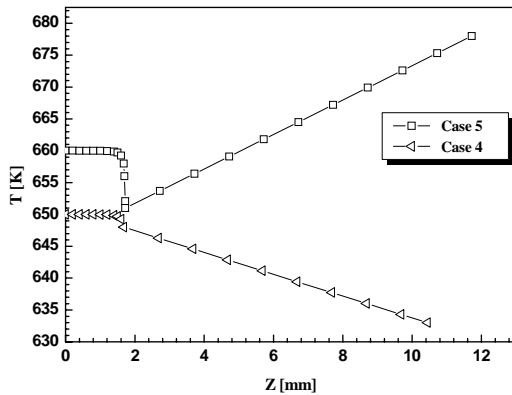


Fig. 14 Variation of jet temperature along the nozzle axis and the jet trajectory centerline.

It is seen from Fig. 13 that both Cases 4 and 5 exhibit a similar trend. Specifically, a sudden drop of pressure occurs inside the nozzle, and then the jet pressure decreases slowly from the nozzle exit to the end of the trajectory. For the jet temperature

variation, on the other hand, Fig. 14 shows a sudden drop of temperature occurring inside the nozzle, followed by a increasing (decreasing) trend from the nozzle exit to the end of the trajectory for the case of $T_a > T_2$ ($T_a < T_2$).

Based on the variations of temperature and pressure given by Figs. 13 and 14, it can mark the complete phase transition process on a phase diagram, as shown in Fig. 15 for Cases 4 and 5. As discussed earlier, kerosene state in the nozzle depends on the injection parameters, while the final fuel state depends on the crossflow conditions. It is seen from Fig. 15 that although the injection state of Case 5 is supercritical, the fuel state at the nozzle exit becomes subcritical. Furthermore, Fig. 15 suggests that the behavior of supercritical and subcritical kerosene injection into an elevated pressure and temperature crossflow was close to the case with a gas jet injecting into a gas crossflow than the liquid jet.

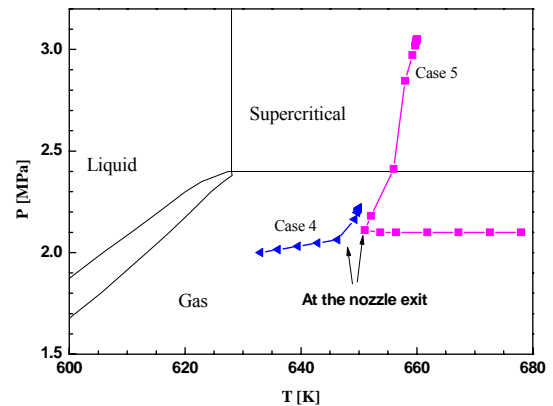


Fig. 15 Phase transition processes of kerosene jet at varying injection pressures and temperatures.

CONCLUDING REMARKS

The jet penetration distances and phase transition processes of supercritical and subcritical RP-3 aviation kerosene injected into a high temperature and pressure crossflow were investigated experimentally over a range of injection and crossflow conditions. Based on a three-component kerosene surrogate, a one-dimensional analysis was proposed and conducted to calculate the fuel flow parameter variation in the nozzle and along the jet penetration trajectory. These analytical results in conjunction with the calculated phase diagram provided insights into the phase transition processes of supercritical and subcritical kerosene jets into a crossflow of elevated temperature and pressure.

It was found that the behavior and penetration distance of supercritical kerosene injection into high temperature and high pressure crossflow were neither the same as those of liquid kerosene injection nor superheated kerosene injection into a crossflow of normal temperature and pressure. The phase transition process results for both supercritical and subcritical

injection cases further showed that since the fuel state at the nozzle exit was subcritical, the resulting behavior and penetration distance were closer to the injection of a gas jet into a gas crossflow than the liquid jet. In spite of similarity, the present trajectory results did not follow the correlation of gas jet. Further investigation for understanding different injection processes is warranted.

ACKNOWLEDGMENTS

The current research program has been supported by the 111 Project Grant NO. B08009.

REFERENCES

- [1] Edwards, T., "USAF Supercritical Hydrocarbon Fuels Interests," AIAA Aerospace Sciences Meeting, AIAA Paper 93-0807, 1993.
- [2] Lin, G.C., Cox-Stouffer, S.K., and Jackson, T.A., "Structures and Phase Transition Processes of Supercritical Methane/Ethylene Mixtures Injected into a Subcritical Environment," *Combustion Science and Technology*, Vol. 178, 2006, pp. 129-160.
- [3] Shih, W-P, Lee, J.G., and Santavicca, D.A., "Stability and Emissions Characteristics of a Lean Premixed Gas Turbine Combustor," *Twenty-Sixth Symposium (International) on Combustion*, 1996, pp. 2771-2778.
- [4] McDonell, V.G., Arellano, L., Lee, S.W., and Samuelsen G.S., "Effect of Hardware Alignment on Fuel Distribution and Combustion Performance For a Production Engine Fuel-Injection Assembly," *Twenty-Sixth Symposium (International) on Combustion*, 1996, pp. 2725-2732.
- [5] Lefebvre, A.H., "The Role of Fuel Preparation in Low Emissions Combustion," *ASME 95-GT-465*, Proceedings of the International Gas Turbine and Aeroengine Congress and Exposition, June 5-8, 1995.
- [6] Yang, V., "Modeling of Supercritical Vaporization, Mixing and Combustion Processes in Liquid-Fueled Propulsion System," *Proceeding of the Combustion Institute*, Vol. 28, 2000, pp. 925-942.
- [7] Edwards, T., and Maurice, L.Q., "Surrogate Mixtures to Represent Complex Aviation and Rocket Fuels," *Journal of Propulsion and Power*, Vol. 17, 2001, pp. 461-466.
- [8] Chen, K.D., "Heat Transfer, Fouling, and Combustion of Supercritical Fuels," University of Iowa, F49620-92-J-0462, 1994, pp. 6-25.
- [9] Yang, V., Hsieh, K.V., and Shuen, J.S., "Supercritical Droplet Combustion and Related Transport Phenomena," AIAA Paper 93-0812, 1993.
- [10] Wu, P.K., Chen, T.H., Nejad, A.S., and Carter, C.D., "Injection of Supercritical Ethylene in Nitrogen," *Journal of Propulsion and Power*, Vol. 12, NO. 4, 1996, pp. 770-777.
- [11] Wu, P.K., Shahnam, M., Kirkendall, K., and Carter, C.D., "Expansion and Mixing Processes of Underexpanded Supercritical Fuel Jets Injected into Superheated Conditions," *Journal of Propulsion and Power*, Vol. 15, No. 5, 1999, pp. 642-649.
- [12] Dounghip, T., Erivin, J.S., Williams, T.F., and Bento, J., "Studies of Injection of Jet Fuel at Supercritical Conditions," *Industrial and Engineering Chemistry Research*, Vol. 41, 2002, pp. 5856-5866.
- [13] Stenzler, J.N., Lee, J.G., and Santavicca, D.A., "Penetration of Liquid Jets in a Crossflow," AIAA 2003-1327.
- [14] Wu, P.K., Kirkendall, K.A., and Fuller, R.P., "Breakup Processes of Liquid Jets in Subsonic Cross flows," *Journal of Propulsion and Power*, Vol. 13, No. 1, January-February 1997, pp. 64-73.
- [15] Wu, P.K., Kirkendall, K.A., and Fuller, R.P., "Spray Structures of Liquid Jets Atomized in Subsonic Crossflows," *Journal of Propulsion and Power*, Vol. 14, No. 2, March-April 1998, pp. 173-182.
- [16] Corn, M., Cohen, J., Hautman, D., Thawley, S., Brown, C., and McDonell, V., "Characterization of A Superheated Fuel Jet in A Crossflow," GT2009-59358, presented at the ASME Turbo Expo, Orlando, Florida.
- [17] Wang, D., and Yu, G., "Investigation of Kerosene Jet Spray in Supersonic Combustion," *Journal of Experiments in Fluid Mechanics*, Vol. 19, No. 2, Jun., 2005, pp. 11-13.
- [18] Kush, E.A., Jr., and Schetz, J.A., "Liquid Jet Injection into Supersonic Flow," *AIAA Journal*, Vol. 11, No. 9, 1973, pp. 1223-1224.
- [19] Tambe, S.B., Jeng, S.M., Mongia, H., and Hsiao, G., "Liquid Jets in Subsonic Crossflow," AIAA 2005-731, presented at the 43rd AIAA Aerospace Sciences Meeting and Exhibit, Reno, Nevada.
- [20] Chen, T.H., Smith, C.R., and Schommer, D.G., "Multi-Zone Behavior of Transverse Liquid Jet in High-Speed Flow," AIAA Paper 93-0453, 1993.
- [21] Lefebvre, A.H., *Gas Turbine Combustion* (2nd ed.), Philadelphia: Taylor & Francis, 1999.
- [22] Ji, C., Enoch, D., Wang, Y.L., Wang, H., and Egolfopoulos, F.N., "Propagation and Extinction of Premixed C₅-C₁₂ n-Alkane Flames," *Combustion and Flame*, Vol. 157, No. 2, 2010, pp. 277-287.
- [23] Dagaut, P., "On the Kinetics of Hydrocarbon Oxidation From Natural Gas to Kerosene and Diesel Fuel," *Phys. Chem. Chem. Phys.*, Vol. 4, 2002, pp. 2079-2094.
- [24] Ely, J.F., and Huber, M.L., "NIST standard Reference Database 4 - NIST Thermophysical Properties of Hydrocarbon Mixtures," National Institute of Standards, Gaithersburg, MD, Feb. 1990.